Hybrid Approach Combining Modelling and Measurement for Fatigue Damage Estimation of Welded Connections in Bridges

Jalil Kwad [ab]* and Prakash Kripakaran[a]

[a] *University of Exeter, College of Engineering, Mathematics and Physical Sciences, Vibration Engineering Section, North Park Road, EX4 4QF, +44 (0)1392 72 6421, Exeter, United Kingdom,*

[b] *Civil Engineering Department, University of Anbar, Ramadi, Anbar, Iraq*

* *Jalil Kwad, jeek201@exeter.ac.uk*

Hybrid Approach Combining Modelling and Measurement for Fatigue Damage Estimation of Welded Connections in Bridges

The fatigue life of structural steel bridges is governed by the time history of in-situ stresses at its fatigue-critical structural details under service conditions. However, these stresses are often not directly and accurately measurable due to the complex geometry of the detail or due to access restrictions. This paper proposes a novel methodology to address this challenge. The methodology infers stresses at fatigue-critical locations by combining in-situ strain measurements taken further away from a critical location in a full-scale bridge. Strains measured at various points around the physical welded connection are used to compute the forces and moments applied at the connection. These forces are then applied to a finite element model of the connection to predict the stresses that are required to evaluate the hot spot stresses. The developed methodology is illustrated for a welded connection in a full-scale bridge. Results show that the predicted time history of hot spot stress is accurate and much more realistic than those obtained from numerical simulations. Also, the study demonstrates that the proposed methodology is applicable for interpreting measurements from full-scale bridges and can be integrated within a measurement interpretation platform for continuous bridge monitoring.

Keywords: Steel bridges; structural health monitoring; fatigue damage; hot spot stress; numerical modelling

Introduction

Metallic bridges of all ages, including those that are approaching or have exceeded their design service life and those that are relatively new having been built over the last few decades, are vulnerable to fatigue damage. Fatigue damage is progressive damage due to cyclic loading and is a concern mainly at locations of high stresses such as connections in civil structures (Sun et al., 2019). Fatigue risk is particularly high for old bridges due to a combination of much greater traffic volumes in recent years and significant age-related deterioration (Marques et al., 2018; Zhou, 2006). A comprehensive survey by Olofsson et al. (2005) examining the age profile of existing steel railway bridges in

Europe shows that more than 70% of these bridges are over 50 years old, and about 30% of them are over 100 years old. The UK has over 6,000 metallic bridges, which are over 50 years old, with fatigue as the principal risk to their structural integrity (Adasooriya et al., 2014). Thus, the reliable assessment of the remaining fatigue life of steel bridges is of great importance both nationally and internationally for making decisions regarding rehabilitation and replacement of existing bridges (Yang et al., 2018;Yan et al., 2017).

Significant research has gone toward evaluating effectively and accurately the remaining fatigue life of metallic bridges. These have focused on evaluating the stress time history induced by loading, and then using it to evaluate the cumulative fatigue damage using an established damage model such as Miner's rule (Miner, 1945) and relevant S-N curves derived from laboratory fatigue tests. The majority of the current approaches rely on fatigue design rules to derive the stress time histories and have two key limitations (Zhou et al., 2007; Wang et al., 2015). First, these approaches are based on the nominal stress, which does not take into account the local stress concentration effects in a specific weld detail (Park et al., 2014). These approaches are hence unreliable, particularly for large structures with complex details for which accurately estimating the nominal stress is often difficult (Ye et al. 2012). Second, current approaches exaggerate greatly the actual applied live loads and in turn the stress cycles, resulting in overly conservative estimates of the remaining fatigue life (Lee et al., 2016; Kashefi et al. 2010). For many bridges, these approaches even give a remaining fatigue life that is negative implying that the bridge has theoretically failed in fatigue while in reality the structure is still in service without any visible evidence of fatigue cracking (Kwon et al., 2012). The unnecessary retrofits or repairs necessitated by such conservative assessment procedures significantly increase bridge maintenance costs (Rashidi et al., 2011).

An alternative method proposed in several standards such as Eurocodes is the hot spot stress approach. It is applicable particularly to connections for which the nominal stress cannot be evaluated accurately because of geometric and/or loading complexities (Chen et al., 2016; Liu et al., 2014; Melaku et al., 2017). This is typical in many welded connections in metallic bridges, which is the primary focus of this paper although presented ideas are applicable also to other types of connections. It should however be noted that the hot spot stress method is not applicable in certain geometrical scenarios, and local approaches based on finite element method such as the effective notch method may be used in such cases. As the focus of this paper is on the hot spot stress method, these local approaches are not discussed here.

The International Institute of Welding (IIW) (Hobbacher, 2016) prescribes rules and recommendations on the process of computation of the hot spot stress through modelling. The hot spot stress approach has two key advantages over the nominal stress methods. First, it explicitly accounts for stress concentration effects in the locality of the weld toe by considering the construction details of the connection. Second, the reduced stress scatter in plates thinner than 25mm implies that only a small number of S-N curves, corresponding to only the different weld types are required for fatigue life evaluation, as the construction details of the connection are already considered in the hot spot stress evaluation. However, this approach still results in overly conservative estimates of remaining fatigue life since it uses design daily traffic loads which are often much larger than those from actual traffic on bridges (Aygül et al., 2012). For plates with thicknesses larger than 25 mm, the application of both nominal stress and hot spot stress methods can be challenging due to the difficulty in accounting for size effects.

With recent advances in sensing technology, in-situ strain measurements have been increasingly employed for assessing the remaining fatigue life of steel bridges

(Helmerich et al., 2007; Zhou et al., 2007). These have been shown to be more reliable than assessments based on stress predictions purely from numerical simulations (Ye et al., 2012; Lee et al., 2016; Schumacher et al., 2006). However, most studies rely on measurements of nominal stress in a main member rather than the local, concentrated stress at a weld detail (Cardini & DeWolf, 2009; Kwon et al., 2012; Seo, Phares, Lu, Wipf, & Dahlberg, 2013). The influence of local (i.e., concentrated) stresses is only indirectly taken into account by using S-N curves that are obtained via experimental testing for specific weld details. There is also the possibility of the structural detail and load type not falling under one of the design classes provided in the codes. In such a scenario, bespoke laboratory tests may be required to generate the S-N curves and this can be a challenge since the testing procedure is expensive and time consuming.

Other studies have attempted to obtain nominal strains and stresses farther away of a fatigue-critical locations (Ni et al., 2010). The nominal stresses are multiplied by a Stress Concentration Factor (SCF) to take into account the stress concentration and dimension effects. This approach is known as a modified nominal stress method in many codes and standards such as Eurocodes (EN 1993-1-9 2005). Pasquier et al. (2016) proposed a methodology that enables evaluating hot spot stresses in hollow section joints using finite element models of the bridge that were identified based on measurements from static load tests. These models were used to predict internal stresses, namely axial, shear and bending stresses in the bridge elements, for traffic loads detected using a weigh in-motion (WIM) system. The predicted stresses were then used to compute hot spot stresses through stress amplification with SCFs. However, computing the SCFs, which determine directly the reliability of the modified nominal stress method, is not straightforward. A recent comprehensive review by (Saini et al., 2016) examining SCFs of welded joints of metallic structures concluded that accurately computing these

parameters is difficult due to their dependence on loading conditions which are generally unknown. Schumacher et al. (2006) showed that SCF values are typically conservative using the case of tubular joints. Moreover, since the stresses were not measured in-situ but predicted through models of the bridge, effects of modelling uncertainties such as environmental conditions (e.g. temperature) and local conditions such as actual speed and location of vehicle, and road profile may persist.

This paper proposes a novel methodology for evaluating in-situ hot spot stress histories that overcomes the above-mentioned drawbacks. It integrates field measurements of strains taken from around a welded plate detail with a numerical model of the connection to evaluate the in-situ hot spot stresses. The measured strains are used to compute the axial, shear and bending forces that are applied to the connection. By applying these forces to the model, it will capture the local effects such as dynamic amplification of load that play a major role in fatigue life. Also, unlike the modified nominal stress method, knowledge of the SCF is not required but its effect is instead explicitly accounted for within the modelling process. This paper investigates the proposed methodology on a fatigue-sensitive welded detail (web-gap) in a specific full-scale bridge.

The paper is organised as follows. It first describes the hot spot stress approach as used in current practice. Then it presents the novel methodology and explains how it can support reliable evaluation of the hot spot stresses. The methodology is subsequently illustrated using strain measurements from the Bascule Bridge in Exeter/UK.

Hot spot stress approach

A comprehensive description of the hot spot stress approach is given in (Lee et al., 2010) and (Hobbacher, 2009). In this paper, only a brief description of this approach, as required to understand the proposed methodology, is given.

Hot spot stress: A location in a welded detail where fatigue cracking is most likely to initiate (e.g. due to abrupt structural discontinuity) is commonly called a hot spot. The stress at this location is referred to as the hot spot stress. The onset of fatigue failure at a hot spot is determined by the time history of hot spot stresses. In a welded connection, hot spots are usually at weld toes. The stress at the weld toe including the nonlinear notch effects is referred to as the notch stress. The notch stress, can be decomposed into three components: membrane stress σ_{mem}, shell bending stress σ_{ben}, and a nonlinear stress component σ_{nlp} due to the weld toe singularity. The hot spot stress includes only the linear stress components - σ_{mem} and σ_{ben}, and can be obtained from in-situ strain measurements or through numerical modelling. The nonlinear stress component σ_{nlp}, is included indirectly when using S-N curves that are obtained from laboratory fatigue tests (Radaj, 1990) for each weld type/local geometry to estimate the fatigue life.

Evaluation of hot spot stress: The International Institute of Welding (IIW) recommends consideration of stresses at two types of hot spots - type *a* and type *b*. Figure 1 shows the two types of hot spots in some typical weld details. Type *a* corresponds to hot spots on the plate surface, and *b* corresponds to those on the plate edge. The hot spot stress at these locations can be obtained using either surface stress extrapolation or linearization of stress in the through thickness direction (Niemi et al., 2006). Due to their relative ease of application, surface stress extrapolation methods are more popular in practice and are also employed in this study. In surface stress extrapolation methods, the hot spot stress is evaluated using the strains measured at certain reference locations adjacent to the hot spot. To avoid nonlinearities, these locations are located outside of the region affected by the weld toe notch singularity.

[Inserting Figure 1 approximately here]

For hot spots of type *a* on a plate having thickness *t*, the hot spot stress $\sigma_{hs,a}$ is computed as shown below through linear extrapolation of the stresses, $\sigma_{0.4t}$ and $\sigma_{1.0t}$, predicted at distances 0.4*t* and 1.0*t* respectively away from the weld toe (Figure 2).

$$\sigma_{hs,a} = 1.67\sigma_{0.4t} - 0.67\sigma_{1.0t} \quad (1)$$

The hot spot stress $\sigma_{hs,b}$ for locations of type *b* is computed using a linearized approximation of a quadratic stress profile that is represented by the stresses - σ_{4mm}, σ_{8mm} and σ_{12mm}, predicted on the plate edge at distances 4mm, 8mm and 12mm respectively from the weld toe. The corresponding equation is as follows.

$$\sigma_{hs,b} = 3\sigma_{4mm} - 3\sigma_{8mm} + \sigma_{12mm} \quad (2)$$

In contrast to the stress profiles for hot spots of type *a*, the stress profile near the weld toe for a hot spot of type *b* is independent of the thickness of the plate, and hence Equation (2) hence does not have any terms related to *t*. However this equation is applicable only as long as the plate thickness is less than 25 mm. When evaluating $\sigma_{hs,b}$ for welded joints with plate thicknesses larger than 25mm, an empirical thickness correction factor that diminishes the fatigue strength also needs to be included (Niemi et al., 2006).

[Inserting Figure 2 approximately here]

Proposed methodology

This study proposes a hybrid methodology for deriving the in-service hot stress time-history through a combination of in-situ strain measurements and numerical modelling. This methodology, which is illustrated in Figure 3, is based on the approach proposed in Kwad et al. (2017), and works broadly as follows.

For a given steel bridge, the first step is to identify its fatigue-critical connections. This can be done using a global finite element model (FEM) of the bridge that is validated using a controlled load test. Then local FEMs are developed for the identified fatigue-critical connections. The local FEMs are linear elastic models that comprise all the connection components (e.g. stiffener, weld) along with small portions of the structural elements that are part of the connection. For example, the local FEM of a main beam-cross beam connection, which is the type of connection investigated in this paper, will include small portions of the intersecting beams in addition to the connection components. Simultaneously a field measurement plan is developed and implemented for the fatigue-critical connections. The measurement plan will include installing strain gauges on the structural elements relevant to the connection in a manner that will enable evaluating the time history of internal forces that are transferred via the connection. These force time histories are then applied to the local FEM to evaluate the time-histories of stresses at relevant locations as necessary to compute the hot spot stress time histories using Equations (1) and (2). These stress time histories are then used for fatigue damage assessment using existing methods. Thus, in principle, if the strain gauges are left to collect measurements continuously, then the fatigue life of the critical details can be monitored continuously via this approach.

[Inserting Figure 3 approximately here]

The key elements in the methodology are now explained in detail.

Global FEM: This is a numerical model of the full-scale bridge that is capable of predicting accurately its global deformation response. This model may be derived initially using structural drawings of the bridge, and later updated and validated using measurements from field testing.

Local FEM: This model essentially simulates the structural behaviour of the connection and includes therefore the connection and the structural elements that intersect at the connection. In this study, the structural elements are main beams and cross beams. These are not modelled fully but only a short length as required to ensure stress concentration effects from the connection are absent at the boundaries.

The local FEM is created according to the IIW recommendations (Niemi et al., 2006) on the application of the hot spot stress approach. The IIW recommends the use of 8-noded shell or 20-noded solid elements, both of which allow for a linear stress distribution through the thickness. The element mesh in the area close to the hot spot must be refined to a degree such that the local stress gradients are captured accurately. Also, the mesh should have nodes at locations where stresses are required according to Equations (1) or (2). If shell elements are used, the weld geometry is usually omitted from the model even though this simplification may underestimate the stiffness of the weld. The stress at a reference location as required for Equations (1) and (2) is either

(1) the predicted maximum principal stress at the corresponding location in the model if the stress vector is oriented within 60^{o} of the normal to a weld toe, or else
(2) the normal stress that is oriented in the direction normal to the weld toe.

Defining suitable boundary conditions for the local FEM is critical to ensure model predictions are reliable. This study evaluates three different boundary conditions and their influence on the performance of the overall methodology (see Section *Local FEM*).

Deployment of monitoring system: Measuring strain histories for fatigue life assessment require a modern data acquisition system with sufficient data storage and a high sampling rate (~100 Hz) to capture dynamic effects of loading. Strain gauges also have to be

installed in a manner that will allow evaluating the internal forces at locations corresponding to the boundary of the local FEM. For each beam intersecting at the connection, sufficient number of strain gauges are required to enable computing the three main internal forces - bending moment (about its major axis), axial force and shear force. In main girder – cross beam connections, such as those in plate girder bridges like the Bascule Bridge that is considered as a case study in this paper, torsion and bending effects about the minor axis can be assumed negligible (Håkansson & Wallerman, 2015) due to the following reasons. The cross beams in such bridges are essentially simply supported between the main girders (Haghani, Al-Emrani, & Heshmati, 2012) and therefore impose no torsion on the main girders. Axial forces are also unlikely in the cross beams due to the lack of lateral forces on the bridge; hence there will be negligible minor axis bending effects in the main girder. Consequently, the following two sets of strain gauges will generally suffice: (i) strain gauges at the top and bottom flanges of the cross-section to capture bending effects, and (ii) a rosette near the neutral axis to capture shear effects. Measurements from these gauges will enable computing the exact location of the neutral axis, and subsequently the bending moment, shear force and axial force through simple Euler-Bernoulli beam bending assumptions. For bridges where torsion and minor axis bending effects are significant, additional strain gauges can be used to evaluate the relevant force and moment components.

Hot spot stress evaluation: The internal forces computed for each measurement time-step are applied as loading to the local FEM of the connection. The local FEM is used to predict the stresses at the reference locations as required to compute the hot spot stress σ_{hs} using Equations (1) and (2). Since the local FEM is a linear elastic model with stresses related linearly to the applied loads, individual FEM runs are not required for determining the stresses due to internal forces and moments evaluated from each measurement time-

step. This can be accomplished through the use of load scaling factors (LSF) – $S_{M,i}$, $S_{V,i}$, $S_{A,i}$, which are essentially the stresses produced at a reference location i by an internal force – namely a bending moment M, a shear force V or an axial force A of unit magnitude. The stress $\sigma_{i,j}$ at a reference location i due to the internal forces M_j, V_j and A_j, evaluated for a measurement time step j, is therefore computed by superposing together the individual stresses $\sigma_{M,i,j}$, $\sigma_{V,i,j}$ and $\sigma_{A,i,j}$, produced by the three internal forces, assuming linear behaviour, as shown using the following equations.

$$\sigma_{M,i,j} = M_j S_{M,i} \tag{6}$$

$$\sigma_{V,i,j} = V_j S_{V,i} \tag{7}$$

$$\sigma_{A,i,j} = A_j S_{A,i} \tag{8}$$

$$\sigma_{i,j} = \sigma_{M,i,j} + \sigma_{V,i,j} + \sigma_{A,i,j} \tag{9}$$

$\sigma_{i,j}$ computed at reference locations i for a time step j are used in Equations (1) and (2) to determine the corresponding hot spot stress $\sigma_{hs,j}$. The time history of hot spot stresses is then used to assess fatigue damage using Miner's rule (Miner, 1945) and appropriate S - N curves.

Fatigue damage assessment: The σ_{hs} time history produced is converted into equivalent cyclic stress time history through a cycle counting algorithm. This will enable creating a stress histogram representing the number of stress cycles within various stress ranges. This study uses the well-known Rainflow counting method (ASTM E1049 - 85, 2005). Then suitable S-N curves that describe the fatigue resistance of the detail are adopted from Eurocode 3 (EN 1993-1-9, 2005), British Standard BS 7608:1993 and (IIW 2016).

The fatigue damage D (the total damage from all stresses that are applied to the detail) is evaluated using damage accumulation models. This study uses Miner's (Miner, 1945) linear damage accumulation model as described by the equation below.

$$D = \frac{n_1}{N_1} + \frac{n_2}{N_2} + \frac{n_3}{N_3} + \cdots = \sum_n^k \frac{n_i}{N_i} \leq 1.0 \quad (3)$$

where k is the number of stress ranges considered in the damage accumulation model. n_i is the number of stress cycles falling within stress range $\Delta\sigma_{ri}$ and is obtained using Rainflow counting on the σ_{hs} time history. N_i denotes the number of resisting stress cycles of the detail for stress range $\Delta\sigma_{ri}$ and is determined from the S-N curve relationships in Eurocode 3 (EN 1993-1-9, 2005) as follows.

$$N_i = N_o.\left(\frac{\Delta\sigma_C}{\Delta\sigma_{ri}}\right)^3, \ (N_o = 2 \times 10^6, \ \Delta\sigma_{ri} \geq \Delta\sigma_D) \quad (4)$$

$$N_i = N_o.\left(\frac{\Delta\sigma_C}{\Delta\sigma_{ri}}\right)^5, \ (N_o = 5 \times 10^6, \ \Delta\sigma_L < \Delta\sigma_{ri} \leq \Delta\sigma_D) \quad (5)$$

$\Delta\sigma_C$ and N_o are constants corresponding to the fatigue strength and fatigue life for a stress range $\Delta\sigma_{ri}$ on the S-N curve. $\Delta\sigma_D$ and $\Delta\sigma_L$ are constant-amplitude fatigue limit and fatigue threshold respectively. Fatigue failure is said to occur when D = 1.0. D can also be used to arrive at an estimate of the remaining fatigue life of the component based on the current loading conditions. It should be noted that partial safety factors for fatigue resistance are not considered in this study.

Case study– Bascule Bridge

Bridge description

The Bascule Bridge in Exeter, UK (Figure 4) was built in 1972, and carries the

northbound carriageway of A379, a major trunk road, over the Exeter Canal. It is a movable bridge with lifting hangers, a counterweight and hydraulic cylinders on both sides of the bridge that enable it to be raised and lowered to allow boats to pass through. The bridge supports one-way traffic of significant volume with a posted maximum speed limit of 40 mph. The bridge uses a twin-main beam system that is classified as fracture critical AASHTO (American Association of State Highway and Transportation Officials, 2010) since the fatigue failure of a single connection can lead to bridge collapse or closure of the bridge for repair.

The bridge has a simply supported span of length 17.28m. It consists of two rolled main girders, 17 cross beams and a composite aluminium deck. The cross beams are 8.12 m long and spaced at 970 mm intervals.

[Inserting Figure 4 approximately here]

The total width of the bridge is 8.12 m with two lanes that are 3.35 m wide each and a 2 m wide footway on one side of the bridge. The longitudinal beams and cross beams are steel rolled sections having the cross-section geometries detailed in Table 1. The longitudinal beams are spaced 8.2 m apart.

[Inserting Table 1 approximately here]

The Bascule Bridge has 34 beam – beam connections corresponding to where the 17 cross beams are connected to the two main girders. This type of connection, commonly used in steel girder bridges, is known to be susceptible to distortion-induced fatigue cracking. In each of these connections, double vertical stiffener plates 13 mm thick are welded to the web of the main girder (inside and outside of the web girder) using a fillet weld, and the inside stiffener is connected to the cross-beam via a series of bolts as shown in Figures 5 (a) and (b).

[Inserting Figure 5 approximately here]

Prior to the mid-1980s, steel girder bridges had cross beams that were joined to the main girder via transverse connection stiffeners. The stiffeners were welded to the main girder web but with a gap near the tension flange. This practice was intended to avoid introducing localized strains in the tension flanges that could eventually result in the formation of fatigue cracks. As a result, a small length of the girder web, extending from the extreme edge of the stiffener to the tension flange, was left unsupported as illustrated in the Figure 5 (b). Differential deflection between the main girders of the bridge under live loading results in cross beam either pulling or pushing the girder web (out-of-plane distortion). The consequence is a high level of cyclic secondary stress in the web gap area that eventually will generate fatigue cracking as illustrated in Figure 5 (c). Connor & Fisher (Connor & Fisher, 2006) found that close to 90% of all fatigue cracking problems in steel bridges in the USA were due to out-of-plane distortion of fatigue sensitive details. Fisher and Roy (2015) provide a more detailed discussion on the out-of-plane distortion manifesting in web-gap regions.

Global numerical model of the bridge

A global FEM for the Bascule Bridge using 28,496 nodes and 26,891 shell elements was developed and validated by Kwad et al. (Kwad et al., 2017). Measurement data from a controlled quasi static loading test using a truck of known loading was used to calibrate the global FEM. The model has been shown to provide reliable stress results for both static and dynamic loading (Kwad et al., 2017). Full details of the model are not presented here for reasons of brevity but are available from (Kwad et al., 2017).

Local FEM

The fatigue-critical connection (Figure 6) in the bridge consist of an assembly of a main girder, cross beam and vertical web stiffener. The ANSYS® parametric design language

(APDL) is used to build a local FEM model of the connection. 20-noded solid elements are used, since the weld can be easily modelled with prismatic elements, to model the cross beams, main beams and vertical stiffener. A fine mesh is adopted, and weld geometry is modelled. The welded connection is assumed to be fully rigid within the local FEM. This assumption is acceptable as the large number of heavy bolts and weld in this connection are likely to make the connection behave in a rigid manner (Zamiri Akhlaghi, 2009). To comply with the IIW recommendations (Hobbacher 2016), the size of the elements is 8 mm x 8 mm (i.e. $0.4t \times 0.4t$) at type '*a'* hotspots and 20 mm x 20 mm (i.e. $t \times t$) for adjacent elements where *t* represents the base plate thickness and is equal to 20 mm. Materials are assumed linear elastic and isotropic (Elastic modulus of steel = 205 GPa and Poisson's ratio = 0.3). The local FEM mesh consists of 54,509 elements with a total of 79,081 nodes. The running time for a typical analysis is approximately 5 minutes on a PC with 8 GB of RAM.

[Inserting Figure 6 approximately here]

The connection is designed to transfer forces from the cross beam, which are created by the vehicles traveling on the bridge deck, to the main (longitudinal) girder. These forces are the key determinant of the stresses at the weld in this connection, and the monitoring system is designed to capture these forces. The internal forces – A, V and M, namely, the axial force, shear force and bending moment, that are computed from the measured strain data will be applied as loading to the local FEM and the global FEM as appropriate.

Defining the boundary conditions for the local FEM can be challenging. Therefore, three different boundary conditions that vary in the level of complexity are attempted to evaluate which one simulates closely the real conditions and provides satisfactory balance between accuracy and computational effort.

(1) *BC1*: In *BC1*, the ends of the main girder are modelled as pinned supports. Therefore, all translational and rotational degrees of freedom at the node at the neutral axis on the two ends of the main beam on either side of the connection with cross-beam are fixed. No constraint is applied on the end of the cross beam.

(2) *BC2:* In *BC2*, the ends of the main girder and the cross-beam are assumed to be on supports that offer partial fixity by using 3 translational and 3 rotational springs with stiffness corresponding to the resistance offered by the rest of the bridge. The COMBINE14 spring element available in ANSYS is used to model the springs. The global FEM is used to identify the stiffness of the springs. A coupling technique available in ANSYS is adopted that uses zero point-mass elements as master nodes to translate the stiffness of the springs to all the nodes along the boundaries of the local FEM.

(3) *BC3:* In *BC3*, a well-known shell-to-solid sub-modelling technique available in ANSYS is employed to transfer displacements from the global FEM for the measured internal forces to the local FEM (Alencar, de Jesus, Calçada, & Silva, 2018).

To find the load scaling factors (LSF), stress responses are computed for individual unit internal forces, i.e. 1 kNm, 1 kN and 1 kN. The predicted values of the normal stress component (inner side of the web gap of the main beam) oriented in the normal direction to the weld toe at the reference locations for each of the applied forces (Figure 7), are the LSFs. These forces are applied separately at the end of the modelled cross beam at a distance of 1040 mm from the connection, which coincides with the physical location of strain gauges on the full-scale bridge. Table 2 presents magnitudes of LSFs of the main girder-cross beam connection for the three types of boundary conditions.

[Inserting Figure 7 approximately here]

[Inserting Table2 approximately here]

Field instrumentation of connection

A monitoring system consisting of 8 weldable strain gauges with 5.84 mm (0.72") active grid length, a data logger and a power source is used to collect the strain data. The sensors are installed at locations corresponding to the boundary of the local FEM. The locations of the strain gauges in the connection are indicated in Figures 8 (a) and (b), in which the rivets are not sketched for clarity. The strain gauges SG 3 to SG-7 represent those installed on the cross beam. These are installed to evaluate the internal forces transferred by the weld. SG 8 is the gauges placed on the main beam at distances 400 mm from the vertical stiffener to capture strains developed in the main girder. SG- 1 and SG 2 are the gauges placed at distances 0.4t (8 mm) and 1t (20 mm) from the weld toe at the end of the vertical stiffener. These are the reference locations at which stresses are required to compute the stress at a hot spot of type *a* according to the IIW recommendations. The locations of these gauges on the full-scale bridge are shown in Figure 8 (c).

[Inserting Figure 8 approximately here]

Strain gauges are used to record the response of the bridge to in service live loads at a sampling rate of 2000 Hz for a period of 6 hours. 2000 Hz is a much higher sampling rate than required for this task but this was used as the instrumentation offered this capability. The purpose of the monitoring was to measure directly the strains caused by the site-specific traffic. For visual clarity and to enable comparison between measured and predicted data, the figures in this section and the next however present data for a duration of only 35 seconds when a heavy vehicle passed over the bridge.

Validation of local FEM

Noise in strain measurements is first eliminated using a low-pass filter with a cut-off frequency of 150 Hz as shown in Figure 9. This frequency was, through a trial and error process, identified as the minimum frequency below which filtering would adversely affect the stress peaks caused by the traffic. The trough in the measurements is due to the passage of a heavy vehicle.

[Inserting Figure 9 approximately here]

Filtered strain measurements from sensors SG-1, SG-3 to SG-7 and SG-8 are multiplied by modulus of elasticity of steel (E = 205 GPa) to get the stress response. The calculated stresses from sensors SG-3 to SG-7 are converted into time history of internal forces using Euler-Bernoulli beam theory equations. Figure 10 shows the magnitudes of computed internal forces, namely bending moments, axial and shear forces for the considered 35 second duration. All three internal forces are used in conjunction with the local FEM discussed in section *Local FEM* to determine the stress time history at 8 mm from the weld toe of the connection.

[Inserting Figure 10 approximately here]

These force time histories and the LSFs, discussed in section *Local FEM*, are used in Equations (6) to (9) to predict individual stresses at the two reference locations and main beam location (i.e. location of the SG-8). Figure 11 shows the time history of predicted $\sigma_{8\,mm}$, the stress at the reference location at a distance of 8 mm from the weld toe, when using boundary conditions *BC1*, *BC2* and *BC3* in the local FEM. The figure also presents the time history of measured stresses at this location as computed using strain measurements from sensor SG-1.

[Inserting Figure 11 approximately here]

The plots show that the local FEM is sensitive to the chosen boundary conditions. This sensitivity can be captured by examining the difference between the predicted stresses for the duration when the bridge is crossed by a heavy vehicle. The peak compressive stress obtained using *BC3* in the local FEM is more realistic than predicted using *BC1* and *BC2*. The stresses predicted by the local FEM using *BC1* and *BC2* agree to a certain degree with the experimental measurements with a mean error of only 3.5% and 5.9% over the 35 second period, respectively. However, when using *BC3,* the mean error is only 2.6%.

Strain measurements from sensor SG-8 are also used to resolve the uncertainty in boundary conditions in the local FEM. Figure 12 presents the time history of measured stresses at this location as computed using strain measurements from sensor SG-8. The figure also shows the stresses predicted by the local FEM using *BC1*, *BC2* and *BC3* at the location of the SG-8. The stresses predicted by the local FEM using *BC3* is almost the same as the measured stresses with a mean error of only 2.5% over the 35 second period. However, when using *BC1* and *BC2,* the mean errors are over 59% and 3.8%, respectively.

[Inserting Figure 12 approximately here]

From Figures 10, 11 and 12, it can be concluded that the predicted stress at the weld region is mainly due to shear in the cross beam. Stresses induced by moment in the cross beam are very small and can be neglected for this connection. For the kind of detail analysed in this study, the vertical load (shear) from the cross-beam should typically cause compression on both sides of the girder web. However, the strain measurements show that there is compression on the inside face and tension on the outside face of the web gap of the girder and this is potentially due to distortion effects. Distortion-induced fatigue cracking is a consequence of cyclically applied small and local deformations that

are normally out-of-plane. According to the field measurements, the stress between the connection plate and the web welds is large enough to result in fatigue cracking.

The results also show that the local FEM using boundary condition *BC3* is found to be appropriate for simulating the local stresses induced by real traffic. Using the local FEM with boundary conditions *BC3*, the time history of hot spot stress σ_{hs} is computed for the duration of the monitoring. Strain measurements from sensors SG-1 and SG-2 are used to derive the measured time history of the hot spot stress at the weld toe. The measured and predicted hot spot stress are compared for a 35-second duration when a heavy vehicle passes over the bridge causing significant stress in the connection. These stresses are given in Table 3.

[Inserting Table 3 approximately here]

The results reveal that there is good agreement between the hot spot stresses obtained using the proposed methodology and its counterpart from the measured strain under real-life loading. The mean percentage error in the predicted stress relative to the measured hot spot stress values is calculated, for the chosen 35 seconds as well as the full duration of monitoring (6 hours). It is observed to be less than 4.1% for the selected 35 seconds, and less than 6.96% for the whole monitoring period. The range of these errors is less than the $\mp$10% error ranges given for hot spot stresses obtained based solely on finite element analysis (Heshmati, 2012). Although these errors are in an acceptable range, a sensitivity analysis is conducted and described in the next section to identify the most suitable finite element mesh and element type configuration for this application.

Effects of mesh size: The effect of mesh size can be inferred from computing the hot spot stress as recommended by the BSI standards (BSI, 2014), i.e. using Equation (1). For stress analysis based on measured strains or finite element models of a relatively fine mesh, the BSI standards recommend the use of linear extrapolation of stresses at distances

0.4t (i.e. 8 mm) and 1.0t (i.e. 20 mm) from the weld toe. Using this equation, hot spot stress for different mesh sizes are calculated and compared in Table 4. It is found that the model when using a fine mesh provides accurate results. Table 4 also shows clearly that the plate surface stresses in the web gap region near the stiffener plate are underestimated with a coarse mesh. The Table shows that a mesh composed of 4 mm or 8 mm can be adopted to obtain a reasonable solution to avoid unnecessary complexity and computational effort. Consequently, the local FEM developed in this research successfully evaluates the hot spot stress at the weld toe and is appropriate for simulating the local stress values induced by the real traffic.

[Inserting Table 4 approximately here]

Fatigue damage assessment based on hot spot stress

In this section, we show how the proposed fatigue stress evaluation procedure can become part of a fatigue damage assessment method using the connection in the Bascule Bridge as a case study. As described in section *Validation of local FEM*, the strain time history from SG-3 to SG-7 and local FEM (*BC3* case, 4 mm mesh size) are used to evaluate the hot spot stress at the connection under real traffic loading. Stress cycles are then counted using the Rainflow algorithm (ASTM E1049 - 85 2005). Figure 13 shows the time history of hot spot stresses for the entire 6 hours duration for which monitoring was conducted. Figure 14 shows the stress histogram obtained after using the Rainflow algorithm.

[Inserting Figure 13 approximately here]

[Inserting Figure 14 approximately here]

Fatigue damage assessment requires the S-N curve for the connection. In Eurocode 3 (EN 1993-1-9 2005), the fatigue strength of hot spot stress range is represented by two curves with respect to typical weld detail categories. The category is designated by the fatigue strength $\Delta\sigma_C$ at 2 million cycles. The S-N curve in Eurocode 3

(EN 1993-1-9 2005) is expressed in Equation (4) and (5). Figure 15 shows the S-N curve provided in the Table B.1 Eurocode 3 (EN 1993-1-9 2005) for the detail category 100, which covers connections such as non load-carrying fillet welds in the Bascule Bridge. Using the linear damage accumulation model, as proposed by Miner's rule (Miner, 1945) and expressed in Equation (3), cumulative fatigue damage is then evaluated from the histogram derived from the hot spot stress time history.

[Inserting Figure 15 approximately here]

It should be noted that all stress ranges below the fatigue threshold $\Delta\sigma_L$ are omitted in the damage accumulation. Table 5 contains the damage ratios obtained for each stress range and also the cumulative fatigue damage - 1.25×10^{-5}, for the considered monitoring period.

[Inserting Table 5 approximately here]

Based on the field measurements, the maximum range of hot spot stress – 78 MPa (Table 5), exceeds the CAFL at the instrumented location. Therefore, the longitudinal girder of the bridge must be considered to have a finite fatigue life and the remaining fatigue life of the bridge have to be estimated. As the bridge has been monitored only for a short duration (6 hrs in total), the author acknowledges that the derived stress histogram is not sufficient to evaluate the remaining fatigue life of the bridge (Connor & Fisher, 2006); this requires data from a much longer monitoring duration (at least a week with 24hrs per day). However, the goal here is only to illustrate that the proposed fatigue stress evaluation method can support an approach for fatigue damage assessment, and the measured data is sufficient for this purpose.

Conclusions

This paper investigates the following hypothesis: detailed finite element models of fatigue-critical connections and in-service strain measurements that capture the shear,

flexure, and axial demands of the modelled connections can be combined to estimate accurately the in-situ hot spot. This enables much more reliable assessment of fatigue life than possible by current methods that employ artificial strain histories predicted for code-specified loads. The paper specifically focuses on investigating this hypothesis for the fatigue-sensitive web-gap welded details in ladder-type bridge decks. However, the presented ideas are applicable to riveted/bolted connections in this type of steel bridges. Conclusions from this research are as follows.

(1) The hot spot strains predicted by the proposed hybrid approach of combining measurements with numerical modelling is within 4% of the field measured strains. This demonstrates that the real stresses at fatigue critical details can be evaluated using the proposed methodology.

(2) The choice of boundary conditions plays an important role in the performance of the local FEM. Boundary condition *BC3* that uses the sub-modelling approach to link the global FEM and the local FEM leads to the best stress predictions.

(3) In the Bascule Bridge, the predicted stress at the weld region is mainly due to internal shear forces in the cross beam. The internal moment is found to have a negligible effect on the hot spot stress.

(4) Continuous fatigue monitoring based on the proposed approach can support real-time fatigue damage evaluation in bridges as shown using the Bascule bridge with measurements for one day.

This research is based on data collected from short monitoring periods. Further long-term field monitoring is essential to prove robustness of methodology and to identify the effects of seasonal variations in ambient conditions and loading. Future work in the field of service-life prediction of existing steel bridges should consider inclusion of environmental conditions and existing deterioration such as corrosion. Consideration of

these conditions may improve both the quality and accuracy of remaining fatigue life assessments of existing steel bridges. Investigate ideas to extrapolate fatigue damage results generated for one instrumented connection to other un-instrumented connections through using global response measurements.

Disclosure statement

No potential conflict of interest was reported by the authors.

Acknowledgments

The first author would like to acknowledge the financial support of The Higher Committee for Education Development in Iraq (HCED IRAQ) scholarship reference D11000218. The authors would like to thank the Bridges and Structures team at Devon County Council for sharing data and providing access to the Bascule Bridge.

References

Adasooriya, N. D., & Siriwardane, S. C. (2014). Remaining fatigue life estimation of corroded bridge members. *Fatigue & Fracture of Engineering Materials & Structures*, *37*(6), 603–622. https://doi.org/10.1111/ffe.12144

Alencar, G., de Jesus, A. M. P., Calçada, R. A. B., & Silva, J. G. S. d. (2018). Fatigue life evaluation of a composite steel-concrete roadway bridge through the hot-spot stress method considering progressive pavement deterioration. *Engineering Structures*, *166*(January), 46–61. https://doi.org/10.1016/j.engstruct.2018.02.058

American Association of State Highway and Transportation Officials. (2010). *AASHTO LRFD bridge Design Specifications* (Vol. 280). https://doi.org/10.1111/febs.12237

ASTM E1049 - 85. (2005). Standard Practices for Cycle Counting in Fatigue Analysis 1. *ASTM International, West Conshohocken, PA.*, *85*(Reapproved 2011), 1–10.

https://doi.org/10.1520/E1049-85R11E01.2

Aygül, M., Al-Emrani, M., & Urushadze, S. (2012). Modelling and fatigue life assessment of orthotropic bridge deck details using FEM. *International Journal of Fatigue*, *40*, 129–142. https://doi.org/10.1016/j.ijfatigue.2011.12.015

Brownjohn, J. M. W. (2007). Structural health monitoring of civil infrastructure. *Philosophical Transactions of the Royal Society A-Mathematical Physical and Engineering Sciences*, 589–622. https://doi.org/DOI 10.1098/rsta.2006.1925

Cardini, A., & DeWolf, J. (2009). Implementation of a long-term bridge weigh-in-motion system for a steel girder bridge in the interstate highway system. *Journal of Bridge Engineering*, (December), 418–423. https://doi.org/10.1061/(ASCE)1084-0702(2009)14:6(418)

Chen, S., Grimes, T., Alampalli, S., Chowdhury, M., & Myers, G. (2016). Dynamic testing of a short span rural bridge. *Change*, (February), 42–48.

Connor, R. J., & Fisher, J. W. (2006). Identifying effective and ineffective retrofits for distortion fatigue cracking in steel bridges using field instrumentation. *Journal of Bridge Engineering*, *11*(6), 745–752. https://doi.org/10.1061/(ASCE)1084-0702(2006)11:6(745)

Dong, P. (2001). A structural stress definition and numerical implementation for fatigue analysis of welded joints. *International Journal of Fatigue*, *23*(10), 865–876. https://doi.org/10.1016/S0142-1123(01)00055-X

EN 1993-1-9. (2005). Eurocode 3: Design of steel structures - Part 1-9: Fatigue. *European Committee for Standardization (CEN), Brussels.*

1 Fisher, J. W., & Roy, S. (2015). Fatigue damage in steel bridges and extending their
2 life. *Advanced Steel Construction*, *11*(3), 250–268.
3 https://doi.org/10.18057/IJASC.2015.11.3.1

4 Haghani, R., Al-Emrani, M., & Heshmati, M. (2012). Fatigue-Prone Details in Steel
5 Bridges. *Buildings*, *2*(4), 456–476. https://doi.org/10.3390/buildings2040456

6 Håkansson, J., & Wallerman, H. (2015). *Finite Element Design of Orthotropic Steel*
7 *Bridge Decks*. Chalmers University of Technology.

8 Helmerich, R., Kühn, B., & Nussbaumer, A. (2007). Assessment of existing steel
9 structures. A guideline for estimation of the remaining fatigue life. *Structure and*
10 *Infrastructure Engineering*, *3*(3), 245–255.
11 https://doi.org/10.1080/15732470500365562

12 Heshmati, M. (2012). *Fatigue Life Assessment of Bridge Details Using Finite Element*
13 *Method. Master's thesis*. Chalmers University of Technology.

14 Hobbacher, A. (2016). *Recommendations for Fatigue Design of Welded Joints and*
15 *Components* (Second Edi). Cham: Springer International Publishing.
16 https://doi.org/10.1007/978-3-319-23757-2

17 Hobbacher, A. F. (2009). The new IIW recommendations for fatigue assessment of
18 welded joints and components – A comprehensive code recently updated.
19 *International Journal of Fatigue*, *31*(1), 50–58.
20 https://doi.org/10.1016/j.ijfatigue.2008.04.002

21 Kashefi, K., Zandi, a. P., & Zeinoddini, M. (2010). Fatigue life evaluation through field
22 measurements and laboratory tests. *Procedia Engineering*, *2*(1), 573–582.

https://doi.org/10.1016/j.proeng.2010.03.062

Kwad, J., Alencar, G., Correia, J., Jesus, A., Calçada, R., & Kripakaran, P. (2017). Fatigue assessment of an existing steel bridge by finite element modelling and field measurements. *Journal of Physics: Conference Series*, *843*(1). https://doi.org/10.1088/1742-6596/843/1/012038

Kwad, J., & Kripakaran, P. (2017). Fatigue assessment in steel bridges: Integrating field measurements and numerical modelling to compute hot spot stresses. *SHMII 2017 - 8th International Conference on Structural Health Monitoring of Intelligent Infrastructure, Proceedings*, (December), 894–903.

Kwon, K., Frangopol, D. M., Asce, D. M., Soliman, M., & Asce, S. M. (2012). Probabilistic Fatigue Life Estimation of Steel Bridges by Using a Bilinear S - N Approach. *Journal of Bridge Engineering (ASCE)*, *17*(1), 58–70. https://doi.org/10.1061/(ASCE)BE.1943-5592.0000225.

Lee, J.-M., Seo, J.-K., Kim, M.-H., Shin, S.-B., Han, M.-S., Park, J.-S., & Mahendran, M. (2010). Comparison of hot spot stress evaluation methods for welded structures. *International Journal of Naval Architecture and Ocean Engineering*, *2*(4), 200–210. https://doi.org/10.2478/IJNAOE-2013-0037

Lee, Y. J., & Cho, S. (2016). Shm-based probabilistic fatigue life prediction for bridges based on fe model updating. *Sensors (Switzerland)*, *16*(3). https://doi.org/10.3390/s16030317

Liu, R., Liu, Y., Ji, B., Wang, M., & Tian, Y. (2014). Hot spot stress analysis on rib-deck welded joint in orthotropic steel decks. *Journal of Constructional Steel Research*, *97*, 1–9. https://doi.org/10.1016/j.jcsr.2014.01.012

Marques, F., Correia, J. A. F. O., Jesus, A. M. P. De, Cunha, Á., Caetano, E., & Fernandes, A. A. (2018). Fatigue analysis of a railway bridge based on fracture mechanics and local modelling of riveted connections. *Engineering Failure Analysis*, *94*(January), 121–144. https://doi.org/10.1016/j.engfailanal.2018.07.016

Melaku, A. F., & Jung, K. S. (2017). Evaluation of welded joints of vertical stiffener to web under fatigue load by hotspot stress method. *International Journal of Steel Structures*, *17*(1), 257–264. https://doi.org/10.1007/s13296-016-0088-6

Miner M. (1945). Miner_Cumulative Damage in Fatigue.pdf. *Journal of Applied Mechanics*, *12*(3), A159–A164.

Ni, Y. Q., Ye, X. W., & Ko, J. M. (2010). Monitoring-Based Fatigue Reliability Assessment of Steel Bridges : Analytical Model and Application. *Journal of Structural Engineering*, *136*(12), 1563–1573. https://doi.org/10.1061/(ASCE)ST.1943-541X.0000250

Niemi, E., Fricke, W., & Maddox, S. J. (2006). Fatigue analysis of welded components: Designer's guide to the structural hot-spot stress approach. *IIW Document*, *13*, 1800–1819.

Olofsson, I., Elfgren, L., Bell, B., Paulsson, B., Niederleithinger, E., Sandager Jensen, J., … Bien, J. (2005). Assessment of European railway bridges for future traffic demands and longer lives – EC project "Sustainable Bridges." *Structure and Infrastructure Engineering*, *1*(No.2), 93–100. https://doi.org/10.1080/15732470412331289396

Park, J. Y., & Kim, H. (2014). Fatigue Life Assessment for a Composite Box Girder Bridge. *International Journal of Steel Structures*, *14*(4), 843–853.

https://doi.org/10.1007/s13296-014-1215-x

Pasquier, R., D. Angelo, L., Goulet, J.-A., Acevedo, C., Nussbaumer, A., & Smith, I. F. C. (2016). Measurement, Data Interpretation, and Uncertainty Propagation for Fatigue Assessments of Structures. *Journal of Bridge Engineering*, *21*(5), 4015087–13. https://doi.org/10.1061/(ASCE)BE.1943-5592.0000861.

Radaj, D. (1990). *Design and analysis of fatigue resistant welded structures* (1st Editio). Abington Hall; Abington; Cambridge CB1 6AH; England: Abington Publishing; Woodhead Publishing Ltd;

Rashidi, M., & Gibson, P. (2011). Proposal of a methodology for bridge condition assessment. *Australasian Transport Research Forum 2011 Proceedings*, (September), 1–15.

Saini, D. S., Karmakar, D., & Ray-Chaudhuri, S. (2016). A review of stress concentration factors in tubular and non-tubular joints for design of offshore installations. *Journal of Ocean Engineering and Science*, *1*(3), 186–202. https://doi.org/10.1016/j.joes.2016.06.006

Schumacher, A., & Nussbaumer, A. (2006). Experimental study on the fatigue behaviour of welded tubular K-joints for bridges. *Engineering Structures*, *28*(5), 745–755. https://doi.org/10.1016/j.engstruct.2005.10.003

Seo, J., Phares, B. M., Lu, P., Wipf, T. J., & Dahlberg, J. (2013). Use of structural health monitoring system for assessment of bridge load rating. *Forensic Engineering 2012*, 18–27. https://doi.org/10.1061/9780784412640.003

Sun, B., Xu, Y. L., Wang, F. Y., Li, Z., & Zhu, Q. (2019). Multi-scale fatigue damage

prognosis for long-span steel bridges under vehicle loading. *Structure and Infrastructure Engineering*, *15*(4), 524–538. https://doi.org/10.1080/15732479.2018.1562478

Tveiten, B. W. T., M, X. W., & V, S. B. (2007). Fatigue Assessment of Aluminum Ship Details by Hot-Spot Stress Approach. *ABS Technical Papers*, *135*(November), 13–17. https://doi.org/10.1115/OMAE2011-50201

Wang, C. S., Yen, B. T., Li, H. T., & Duan, L. (2015). Fatigue life evaluation of in-service steel bridges by using bi-linear S-N curves. *Advanced Steel Construction*, *11*(3), 269–282. https://doi.org/10.18057/IJASC.2015.11.3.2

Xiao, Zhi-Gang and Yamada, K. (2004). A method of determining geometric stress for fatigue strength evaluation of steel welded joints. *International Journal of Fatigue*, *26*, 1277–1293. https://doi.org/10.1016/j.ijfatigue.2004.05.001

Yan, D., Luo, Y., Yuan, M., & Lu, N. (2017). Lifetime fatigue reliability evaluation of short to medium span bridges under site-specific stochastic truck loading. *Advances in Mechanical Engineering*, *9*(3), 1–12. https://doi.org/10.1177/1687814017695047

Yang, D. Y., & Frangopol, D. M. (2018). Evidence-based framework for real-time life-cycle management of fatigue-critical details of structures. *Structure and Infrastructure Engineering*, *14*(5), 509–522. https://doi.org/10.1080/15732479.2017.1399150

Ye, X. W., Ni, Y. Q., Wong, K. Y., & Ko, J. M. (2012). Statistical analysis of stress spectra for fatigue life assessment of steel bridges with structural health monitoring data. *Engineering Structures*, *45*, 166–176.

https://doi.org/10.1016/j.engstruct.2012.06.016

Zamiri Akhlaghi, F. (2009). *Fatigue life assessment of welded bridge details using structural hot spot stress method. Master's thesis*. Chalmers University of technology.

Zhou, T. Q., & Chan, T. H. T. (2007). Hot spot stress analysis of fatigue for Tsing Ma Bridge critical members under traffic using finite element method. *Progresses in Fracture and Strength of Materials and Structures, 1-4*, *353–358*(3), 925–928. https://doi.org/10.4028/www.scientific.net/KEM.353-358.925

Zhou, Y. E. (2006). Assessment of Bridge Remaining Fatigue Life through Field Strain Measurement. *Journal of Bridge Engineering (ASCE)*, *11*, 737–744. Retrieved from http://ascelibrary.org/doi/abs/10.1061/(ASCE)1084-0702(2006)11:6(737)

Table 1. Geometrical characteristics of the main girders and cross beams.

Structural element	Depth (mm)	Top flange width (mm)	Top flange thickness (mm)	Bottom flange width (mm)	Bottom flange thickness (mm)	Web thickness (mm)
Main girder	926	304	32	304	32	20
Cross beam	523	208	13	208	13	10

Table 2. Calculated load scale factors (LSFs) for the three types of boundary conditions of the connection

Boundary condition type	Load scale factor (LSF)	Stress (SY) at 8 mm from weld toe $\sigma_{0.4t}$ (MPa)	Stress (SY) at 20 mm from weld toe $\sigma_{1.0t}$ (MPa)
BC1	$S_{M,i}$	0.062	0.064
	$S_{V,i}$	-1.143	-0.470

	$S_{A,i}$	0.105	0.161
BC2	$S_{M,i}$	0.069	0.078
	$S_{V,i}$	-1.410	-0.935
	$S_{A,i}$	-1.710	-0.942
BC3	$S_{M,i}$	0.101	0.220
	$S_{V,i}$	-1.480	-0.980
	$S_{A,i}$	-3.990	-3.200

Table 3. The measured and predicted hot spot stress of the connection when a heavy vehicle passed over the bridge

Connection type	$\sigma_{8\text{mm}}$ from local FEM (MPa)	$\sigma_{20\text{ mm}}$ from local FEM (MPa)	Hot spot stress σ_{hs} based on strain measurements (MPa)	Hot spot stress σ_{hs} based on proposed methodology (MPa)
Vertical stiffener to the beam web	12.00	7.96	14.71	14.10

Table 4: Measured and predicted hot spot stress error comparison of the connection when a heavy vehicle passed over the bridge with different mesh sizes.

Mesh size	Predicted hot spot stress (MPa)	Error (%)
20	6.52	55.60
10	12.66	13.95
8	14.10	4.10
4	14.44	1.84
2	14.54	1.20
1	14.60	1.00
0.5	14.91	-1.40

Table 5: Cumulative fatigue damage (D) evaluated over two days (6 h period).

$\Delta\,\boldsymbol{\sigma_{ri}}$ [MPa]	$\boldsymbol{n_i}$	$\boldsymbol{N_i}$	$\boldsymbol{D = \frac{n_i}{N_i}}$
30	64	42.7E+07	0.15E-06
34	49	22.8E+07	0.21E-06
38	47	13.1E+07	0.36E-06
42	29	79.3E+07	0.37E-06
46	38.5	5.03E+07	0.77E-06
50	45.5	3.32E+07	1.37E-06
54	33	2.26E+07	1.46E-06
58	25.5	1.58E+07	1.61E-06
62	21	1.13E+07	1.85E-06
66	11	0.83E+07	1.32E-06
70	4.5	0.62E+07	0.73E-06
74	10	0.48E+07	2.08E-06
78	5	0.41E+07	1.21E-06
Total Cumulative fatigue damage			1.25E-5

Figure 1: Hot spots of types *a* and *b* (Hobbacher 2016) with the arrows indicating the directions of the loads at the connection.

Figure 2: Evaluation of the hot spot stress at a hot spot of type *a* through linear extrapolation (Hobbacher 2016).

Figure 3: Overview of the proposed methodology for stress time history/fatigue damage evaluation at directly monitored details.

Figure 4: Bascule Bridge overview.

Figure 5: (a) The cross beam is attached to the vertical web-stiffener of the girder by bolts, (b) Layout and dimensions of the cross beam-main girder beam connection and

(c) Differential deflection of bridge girders results in high local bending stresses in unstiffened web gaps.

Figure 6: Local FEM of the fatigue critical connection.

Figure 7: Extrapolation path of considered stresses at web gap region (y-axis represents the vertical direction).

Figure 8: (a) Schematic of weldable strain gauges installed to top, bottom flanges and mid web of cross beam (front view), (b) Schematic showing locations of weldable strain gauges in web gap near weld region of main girder (side view) and (c) Weldable strain gauges installed in web gap near the stiffener (see Figure 5).

Figure 9: Raw strains measured over a 35 second duration by sensor SG-1, and after filtering using a lowpass filter with a cut-off frequency of 150 Hz.

Figure 10: Internal moments and shear forces computed over a 35 second duration using strains from sensors SG-3 to SG-7.

Figure 11: Comparison of the time history (35 sec) of stresses measured by sensor SG-1 with that of stresses predicted by local FEM with boundary condition *BC1, BC2 and BC3.*

Figure 12: Comparison of the time history (35 sec) of stresses measured by sensor SG-8 with that of stresses predicted by local FEM with boundary condition *BC1, BC2* and *BC3.*

Figure 13: Hot spot stress time history (6 h).

Figure 15: SN characteristic curve Detail 100 ($\Delta\sigma_c$ = 100 MPa).

Figure 14: Histogram of measured data – (6 h).

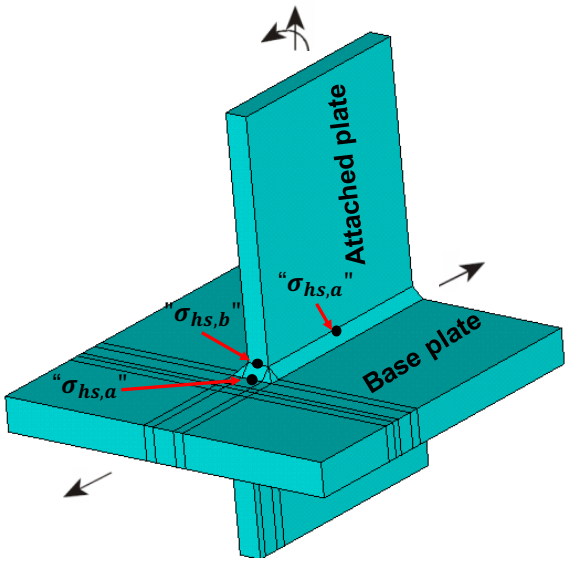

1

2 **Figure 1:**

3

4

5

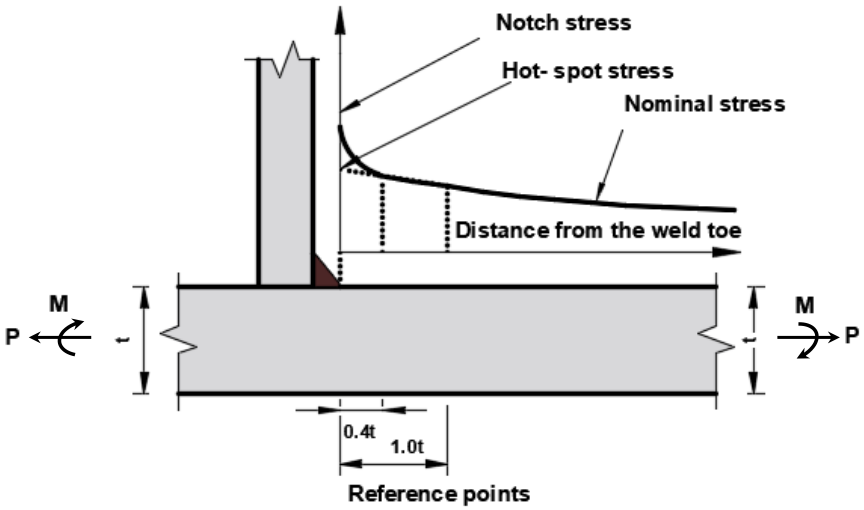

6

7 **Figure 2:**

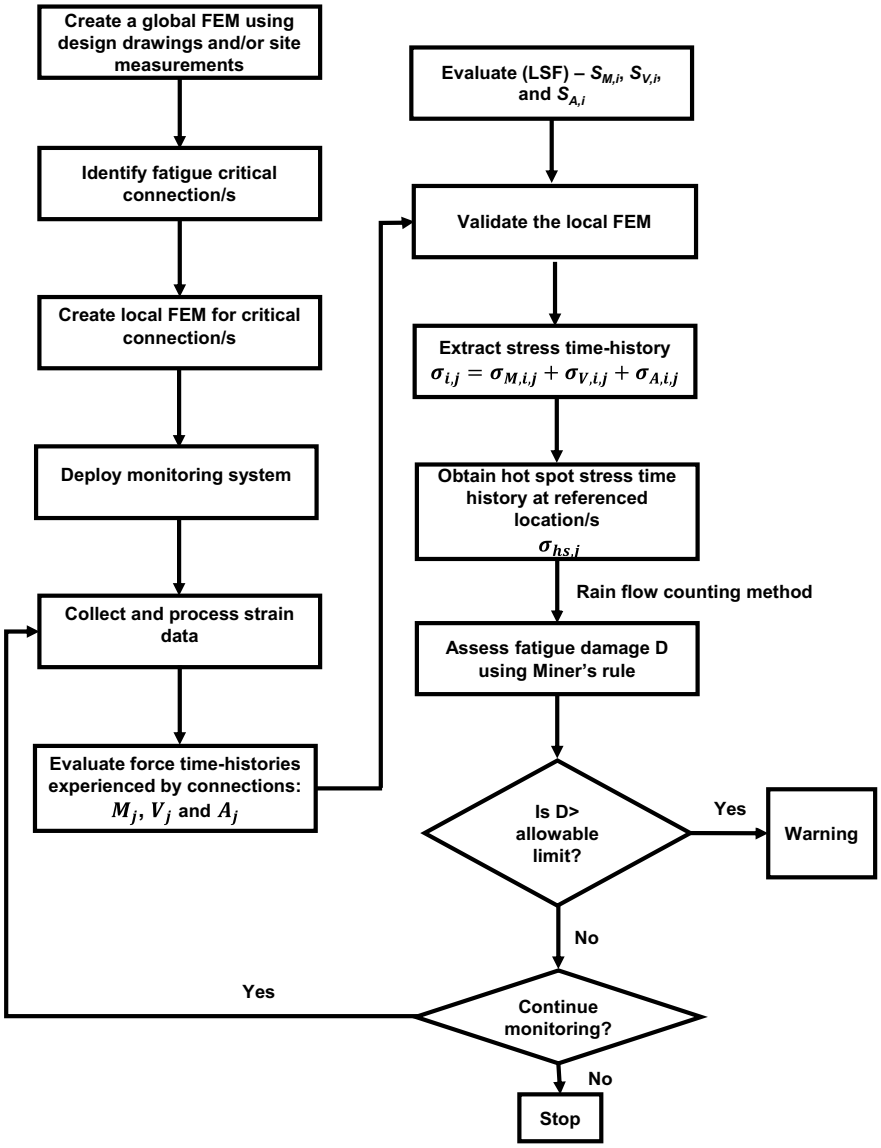

1

2 **Figure 3:**

3

4 **Figure 4:**

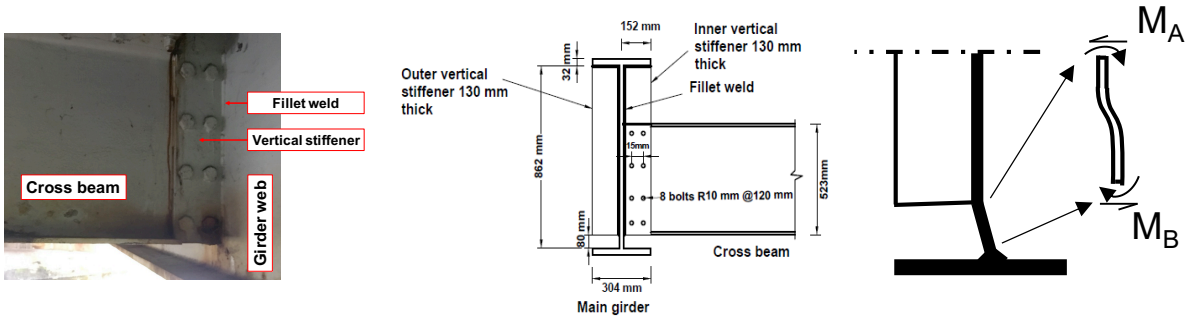

(a) **(b)** **(c)**

1 **Figure 5:**

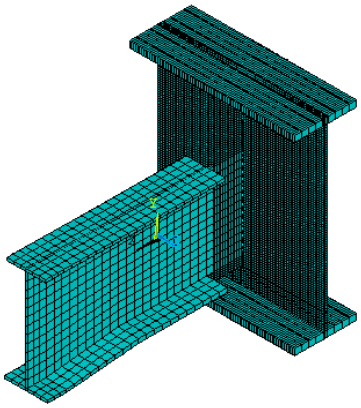

2

3 **Figure 6:**

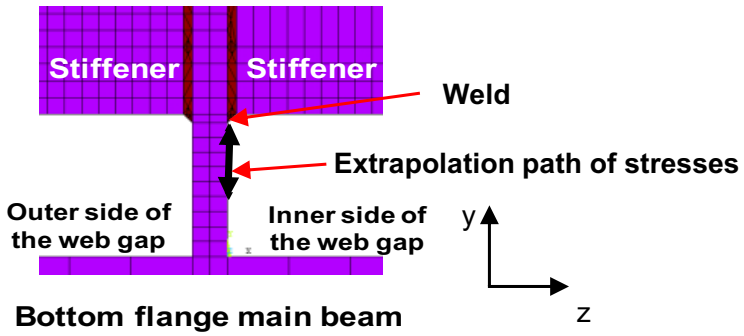

4

5 **Figure 7**:

6

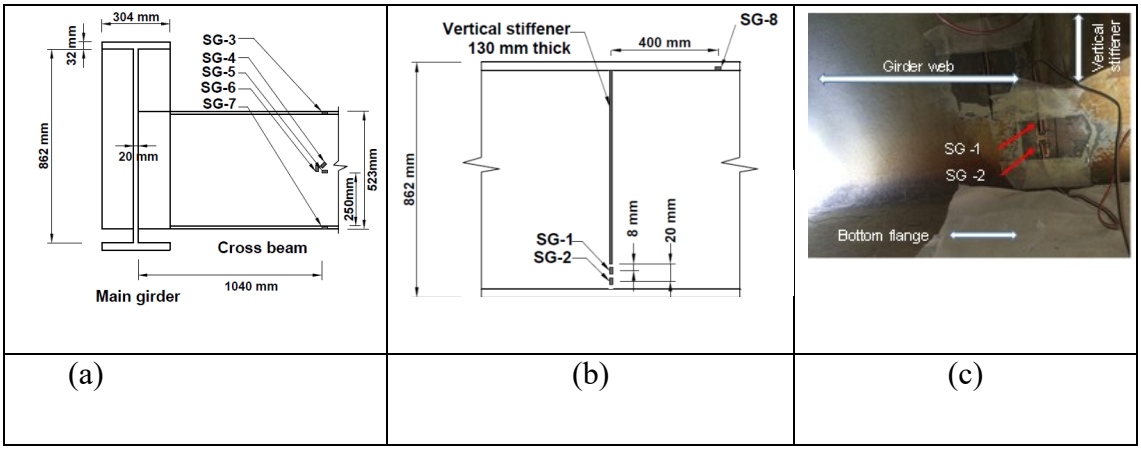

1

2 **Figure 8:**

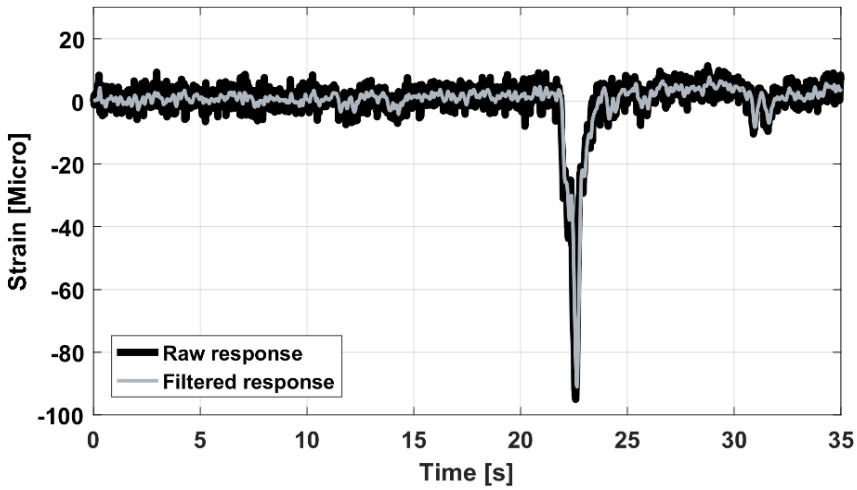

3

4 **Figure 9:**

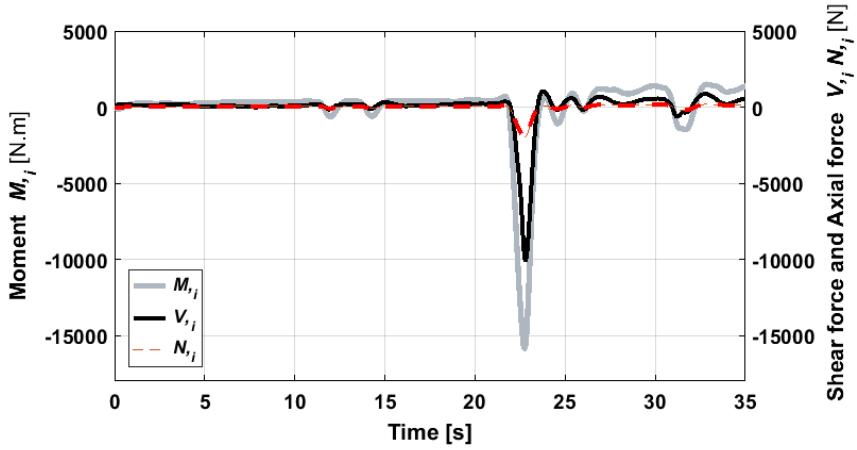

5

6 **Figure 10:**

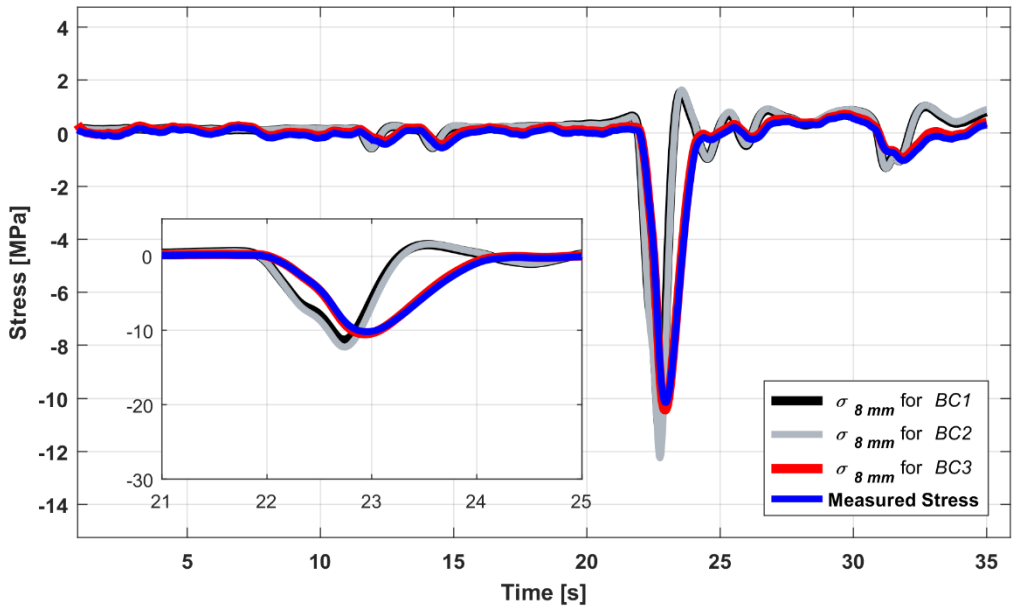

1

2 **Figure 11:**

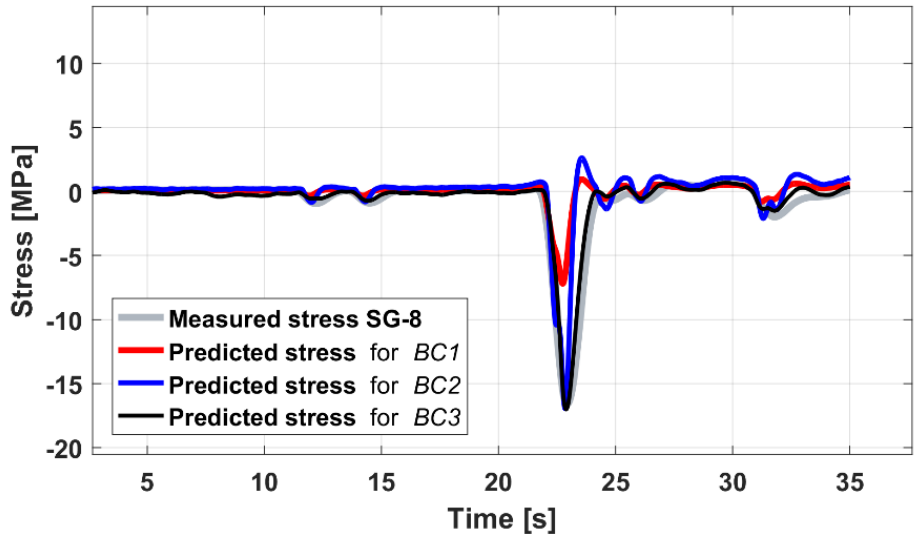

3

4 **Figure 12:**

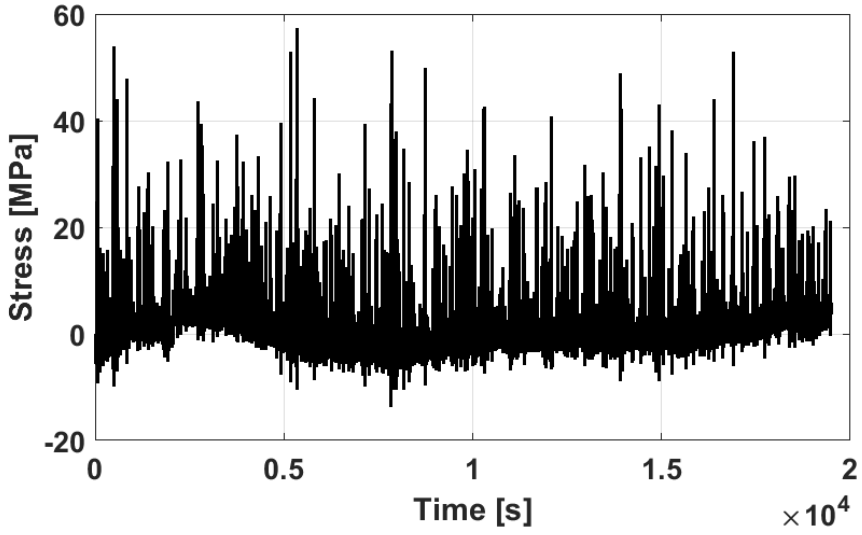

Figure 13:

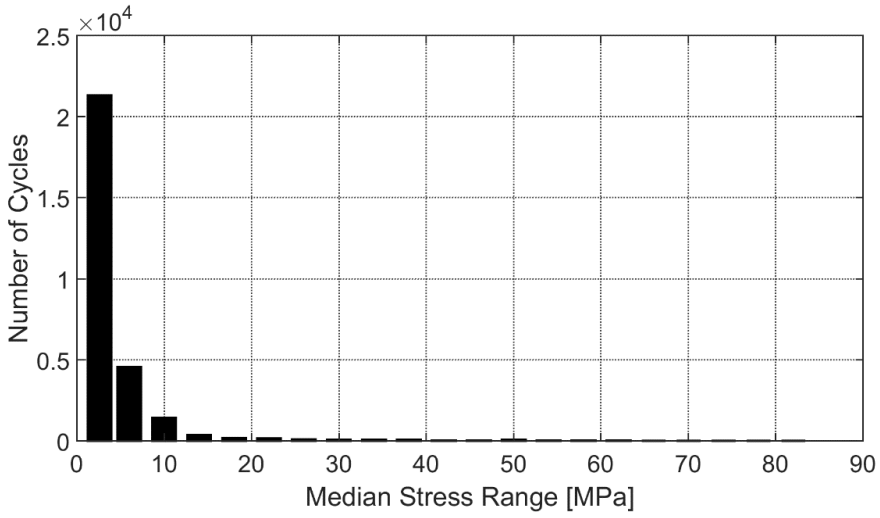

Figure 14:

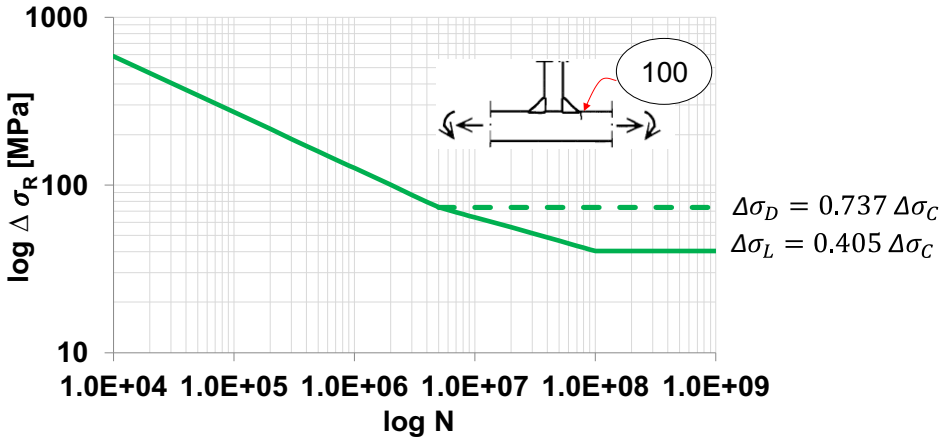

Figure 15: